Chemical Engineering Journal 161 (2010) 234–239

Contents lists available at ScienceDirect

Chemical Engineering Journal

journal homepage: www.elsevier.com/locate/cej

Synthesis of organic nanoparticles in a 3D flow focusing microreactor

Valérie Génot[a,*], Serge Desportes[b], Callie Croushore[a], Jean-Pierre Lefèvre[a], Robert Bernard Pansu[a], Jacques Alexis Delaire[a], Philipp Rudolf von Rohr[b]

[a] PPSM, D'Alembert Institute, CNRS, ENS Cachan, UniverSud Paris, 61 av. Pdt Wilson, 94230 Cachan, France
[b] ETH Zurich, Institute of Process Engineering, Sonneggstrasse 3, Zurich CH-8092, Switzerland

ARTICLE INFO

Article history:
Received 17 December 2009
Received in revised form 2 April 2010
Accepted 15 April 2010

Keywords:
Microfluidic
3D hydrodynamic focusing
Mixing characterization
Organic nanoparticles
Crystallization
Size tuning

ABSTRACT

In this paper, we present the synthesis of organic nanocrystals in a 3D hydrodynamic focusing device through a non-solvent crystallization process. This microreactor was designed in order to control the supersaturation level, while manipulating mixing conditions, and to avoid fouling and clogging within the main channel. Rubrene, the molecule of interest, was dissolved in a THF–ethanol mixture and was injected through a silica capillary. Two side flows containing the non-solvent and the surfactant, water and CTACl respectively, surround and interact with the capillary flow and mixing occurs through diffusion. First, we quantify the water diffusion process within the focused beam by confocal fluorescence microscopy in the presence of fluorescein. It is shown here that the efficiency and the quality of the mixing between the aqueous side flow and the focused organic solution are improved by increasing the side flow rate to the capillary flow rate ratio, i.e. the focusing ratio. Second, the synthesis of rubrene crystals were performed under a variety of flow rate conditions. We show that, by increasing the focusing ratio (from 5 to 40), the mean size of nanocrystals decreases (from 110 to 50 nm). The characterization of the mixing process allows for a better understanding of rubrene nanocrystal synthesis: a fast supersaturation induces the generation of numerous nuclei, which limits the crystal growth. Herein, we show that the 3D hydrodynamic focusing microreactor efficiently produces organic nanoparticles of controlled size, without the deposition of large, unwanted crystals on the microchannel walls.

1. Introduction

Microfluidic technologies have been employed to perform a variety of chemical processes, including organic syntheses, biochemical reactions [1,2], heterogeneous catalysis [3,4], and nanoparticle formation [5,6]. Microreactors provide several advantages in these types of processes when compared to macroscale applications [7,8]. The high surface area to volume ratio, which is two to three orders of magnitude larger than a conventional batch reactor, enhances heat and mass transfer, thus reducing temperature and concentration gradients in microchannels [1,2,8]. Additionally, the laminar flow field developed in such systems improves the reproducibility and allows for the continuous implementation of chemical processes [10]. Moreover, the environmental impact of nanoproduction is minimized because of the decrease in required volume compared to volumes needed for traditional bulk methods. This provides for the ability to use a large range of operating conditions, consuming small amounts of organic compounds, solvent and energy. The relative ease of implementation of optical set-ups, heaters, coolers, sensors, and different processing sections (mixing, reaction, quenching, and separation) allows for online analysis and precise control of the physical conditions of the reaction medium (concentration, temperature, pressure). With reference to these advantages, microfluidic routes have been employed in the continuous production of nanomaterials with controlled properties [9].

Several key parameters determine the size of nanoparticles in wet chemical methods including temperature, mixing efficiency and concentrations of the reagents. The latter two determine the supersaturation conditions, which govern the nucleation and growth kinetics. Several kinds of microreactors have recently demonstrated the ability to precisely control these parameters during the synthesis of quantum dots [11–16], metallic nanoparticles [17–20], oxides [21] and liposomes [22].

Nevertheless, the synthesis in microreactors does face some challenges and the transfer of a flask batch process technology into a continuous flow microreactor is not so obvious. At this small scale, surface forces and surface properties, including surface tension, the physical or chemical interaction(s) between reactants and surface and the roughness of the surface become more significant than the particle motion [9]. This can cause the deposition of nanoparticles or even clogging of the microreactor which can

* Corresponding author. Tel.: +33 (0) 1 47 40 77 38.
E-mail address: genot@ppsm.ens-cachan.fr (V. Génot).

1385-8947/$ – see front matter © 2010 Elsevier B.V. All rights reserved.
doi:10.1016/j.cej.2010.04.029

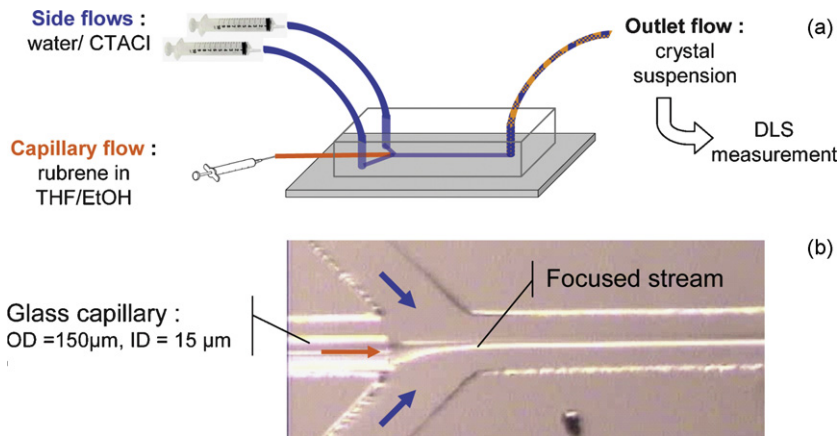

Fig. 1. (a) Y-type microdevice equipped with capillary, inlet and outlet tubing. (b) Magnified picture of the Y junction between the inlet flows. The focused stream appears in the middle of the main channel.

hinder the synthesis of nanoparticles of controlled size. There are certain ways in which microreactor fouling can be prevented. This includes changing the pH of the solutions or surface modification such as silanization, which was reported in the case of metallic particles synthesis [9,19]. Biofouling, in particular, has been shown to be limited by the growth of a poly(ethylene glycol) film on the surface of the microsystem [23].

In addition to preventing the deposition of unwanted nanoparticles, the design of the microreactor is a crucial point to consider in order to achieve faster mixing in a laminar flow regime with a narrow residence time distribution. Research performed on silica nanoparticles showed that the implementation of a mixing section and the reduction of axial dispersion by a segmented two-phase flow improved the monodispersity of the materials [21]. Some other approaches have also addressed these bottlenecks, for example the interdigital mixer [12] or the droplet-based two-phase flow used in quantum dot synthesis [13–15].

It has been shown that 3D fluidic geometries, as well as coaxial flow and 3D hydrodynamic focusing, can overcome the deposition process on the channel walls during a precipitation reaction, as demonstrated for rubrene nanocrystals [24] and for iron oxide nanoparticles syntheses [25]. Due to laminar flow within the microchannels, mixing only occurs by molecular diffusion. For fast reactions like crystallization in a non-solvent which is sensitive to the supersaturation level, reducing and controlling the mixing time in a reproducible manner are challenging. The hydrodynamic focusing technique offers the ability to reduce the mixing time from milliseconds to microseconds [26,27]. Focusing is commonly achieved in microfluidic chips by the combination of the sample stream with sheathing fluid streams. It would be more advantageous to have a true 3D system so that the sample is focused in both the substrate plane and the vertical axis. The advantages from a 3D system include decreasing the stream thickness and limitating the interactions between the sample and the channel walls.

Here, we present a 3D hydrodynamic focusing device which is based on the microfabrication of a Y-type microchannel system moulded in PDMS. A glass capillary is positioned into the intersection of the channels (cross-sectional area: 170 μm × 170 μm). The implemented reaction is the non-solvent crystallization of rubrene. Rubrene nanocrystals are valuable in the field of organic electronics materials [28,29] and the presented microfluidic route appears to us as a promising approach to produce rubrene nanocrystals. Rubrene was also selected because it offers fluorescence properties which have allowed previous investigations by fluorescence lifetime imaging microscopy (FLIM) [24]. The results obtained by FLIM show a strong kinetic effect between the operating conditions and the crystallization process.

The overall aim of this work was to investigate how manipulations of the operating conditions allow for the control of nanoparticle size distributions. Moreover, since the crystallization process and the nanocrystal size are linked to the diffusion dynamics, a quantification of this mixing process was performed. Two main parameters will be described that were used to quantify the performance of a passive mixer, the mixing efficiency and the mixing uniformity. To test these factors, confocal laser scanning microscopy (CLSM) was used for the quantification of diffusion within this 3D hydrodynamic focusing microdevice.

2. Experimental

2.1. Reagents

Rubrene (5,6,11,12-tetraphenylnaphthacene) and fluorescein were purchased from Aldrich and were used as received. Tetrahydrofuran (THF, spectroscopic grade) and absolute ethanol (EtOH, spectroscopic grade) were purchased from SDS. All aqueous solutions were made with deionized water. The surfactant cetyltrimethylammonium chloride (CTACl) was used as a stabilizing agent and was purchased from TCI-Tokyo.

2.2. Device fabrication and its implementation

As previously reported elsewhere [30,31], the microreactor was fabricated by casting PDMS on a silicon wafer that was patterned by photolithography using a spin coated negative photoresist (SU8, MicroChem). Reservoirs were drilled in the cut PDMS block and the PDMS was irreversibly bonded to a glass substrate (76 mm × 26 mm) with oxygen plasma treatment. A glass capillary tube (Polymicro Technologies, OD = 150 μm, ID = 15 μm) was inserted into the microreactor and was fixed with epoxy glue to avoid leakage. The PTFE tubing was inserted into the reservoirs of the PDMS block as illustrated in Fig. 1a. The device was then placed under a binocular microscope to control the stability of the flow and the focusing quality in the main channel.

2.3. Confocal laser scanning microscopy (CLSM)

The efficiency of the mixing and the mixing uniformity within the focused stream were determined using confocal laser scanning microscopy (CLSM 5 Pascal, Zeiss). The excitation of the fluorescent dye, fluorescein, was done by an Argon ion laser at 488 nm wavelength with a high pass filter. For mixing level measurements, the organic and aqueous solutions were respectively water with CTACl (10^{-2} mol L^{-1}) and a THF–ethanol mixture (30/70, v/v) respectively.

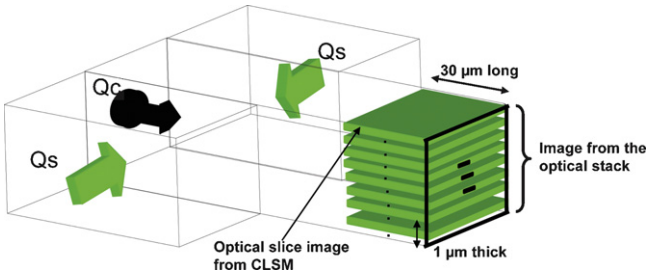

Fig. 2. Scheme of the CLSM imaging at each position along the main channel.

Fluorescein (1.5×10^{-4} mol L^{-1}) was then dissolved equally in the two reference solutions. When flowing these two solutions separately in the microreactor, the fluorescence intensity measured for the aqueous solution was 10 times higher than that of the organic solution [33]. Due to the difference in intensities, the dye acted as a label for the degree of mixing between the water and the organic focused stream. The aqueous solution flowed from the side channels with a volumetric flow rate (Qs) which was varied between 5 and 30 μL min^{-1}. The organic solution flowed from the capillary into the main channel with a volumetric flow rate (Qc) in the range of 1–3 μL min^{-1}.

Using CLSM, a 1 μm thick optical slice was imaged by scanning the channel perpendicularly to the cross-section over the width of the channel and over 30 μm along the channel. The resolution of each slice was 3.3 μm^2 per pixel. The acquisition time for one pixel was 3.6 μs and eight measurements per pixel were averaged for a better representation of the focused stream. All of the images obtained from the PDMS inner surface to the glass substrate at the bottom were stacked and then summed at different positions along the main channel. Each stack allowed us to reconstruct, at each position, an intensity map of the cross-section. The intensity was averaged over the 30 μm length of the stack (Fig. 2).

2.4. Rubrene crystallization

Rubrene was dissolved in a THF/EtOH mixture (30/70, v/v) to reach a concentration of 4.13×10^{-4} mol L^{-1}. The solubility of rubrene in the organic solution is 1.4×10^{-3} mol L^{-1} (0.745 g L^{-1}). This rubrene solution was pumped through the glass capillary inlet at a flow rate (Qc) varying between 0.5 and 3 μL min^{-1}. The capillary was connected to a 500 μL glass syringe positioned in a syringe pump (Model 11 Plus Dual; Harvard Apparatus). The aqueous solution of CTACl, 10^{-2} mol L^{-1} (CMC = 1.3×10^{-3} M [32]) was pumped through each side channel inlet via PTFE tubing at a fixed flow rate (Qs) of 10 μL min^{-1}. Both PTFE tubes were connected to 10 mL plastic syringes set that were placed in an additional syringe pump (Model PHD remote; Harvard Apparatus). Thus, the residence time was close to 2 s.

The solutions collided at a Y junction, forming a focused stream in the main channel. Because of the difference in refractive index between the organic and aqueous solutions, the focused flow clearly appeared under the binocular microscope (Fig. 1b). Mixing occured through diffusion along the channel and induced precipitation.

The rubrene nanoparticle suspension was collected through a PTFE outlet tube. Due to light sensitivity of rubrene, all the solutions containing rubrene and its suspensions were maintained in a brown glass bottles that were wrapped in aluminium foil. For size measurements and further analyses, at least 1.5 mL of suspension was required. Therefore, the sampling time varied between 0.5 and 1.5 h depending on the total volumetric flow rate. During low flow rates and after long running times, undesirable crystals could grow and be detected particularly at the edge of the capillary, resulting in a crystal sheath around the flow coming out of the capillary.

2.5. Size measurements

Each rubrene crystal suspension was analysed from 1 to 5 days after synthesis by Dynamic Light Scattering under a 632.8 nm laser beam (DLS, Zetasizer NanoZS, Malvern Instruments). Each sample was analysed at least 3 times. For each run, the size distribution was given from which the mean size was determined.

3. Results and discussion

3.1. Mixing characterization of the aqueous and organic solutions

In order to calculate the Reynold's number in the microreactor, it was assumed that the mixture is similar to water (density ≈ 1000 kg m^{-3} and viscosity ≈ 10^{-3} Pa s). Therefore, with a mean velocity around 1.25 cm s^{-1}, the flow in the microdevice is laminar as indicated by a Reynolds number close to 2. This is far lower than for a turbulent flow and it can be assumed that mixing between the two side flows within the focused beam is induced by molecular diffusion alone.

Previous studies concerning the preparation of Ag nanoparticles and rubrene nanocrystallization [24] have highlighted that the central stream, where the crystallization takes place, is focused in three dimensions and does not contact the channel walls at any point along the microreactor. Thus, a region of interest (ROI) corresponding to the focused stream was defined at the entrance of the main channel, 300 μm away from the capillary outlet where the laminar flow profile is fully established [34]. The efficiency of the diffusion process was quantified by translating this ROI to different positions along the main channel. This ROI fitted the shape of the focused stream which is mainly determined by the focusing ratio of the volumetric flow rates defined as FocRatio = 2Qs/Qc. Fig. 3 shows a typical reconstruction of the CLSM pictures at different positions: 300, 700, 1300, 1700, 2200, and 2700 μm away from the capillary outlet. The zigzag shape of the fluorescein fluorescence in the ROI, might be attributed to the oscillations created by the pumps which imply the instability of the focused beam as observed under CLSM experiments. The right inset is a numerical magnification of the ROI to give a better visualization of the fluorescence intensity distribution. The relationship between each position (x) and the mean residence time (t_{res}) is described by the following equation:

$$t_{res} = \frac{Ax}{2\,Qs + Qc} \quad (1)$$

where A is the cross-sectional area.

Qualitatively, we can observe that the focused stream has a rectangular shape (dark area), well centred in the channel in regard to its width. The fluorescence intensity in the ROI increases with position along the channel. The mutual diffusion processes control the mixing of the aqueous and organic solutions, which increases the water content within the focused stream, and thus increases the fluorescence intensity of fluorescein therein. Here, the diffusion of the dye, due to its partition ratio between aqueous and organic media, is negligible compared to the diffusion process of the smaller solvent molecules [35].

From each picture in the ROI, the fluorescence emission intensity was measured and an in house Matlab©code was used to determine the degree of mixing, which corresponds to the fraction of water in the aqueous/organic mixture, noted W. From the fluorescence intensity at each pixel, the average fraction (W_{mean}), and its standard deviation (σ) were determined over each analysed ROI. The minimum intensity (I_{min}) and the maximum intensity (I_{max}) were determined by flowing the two reference solutions contain-

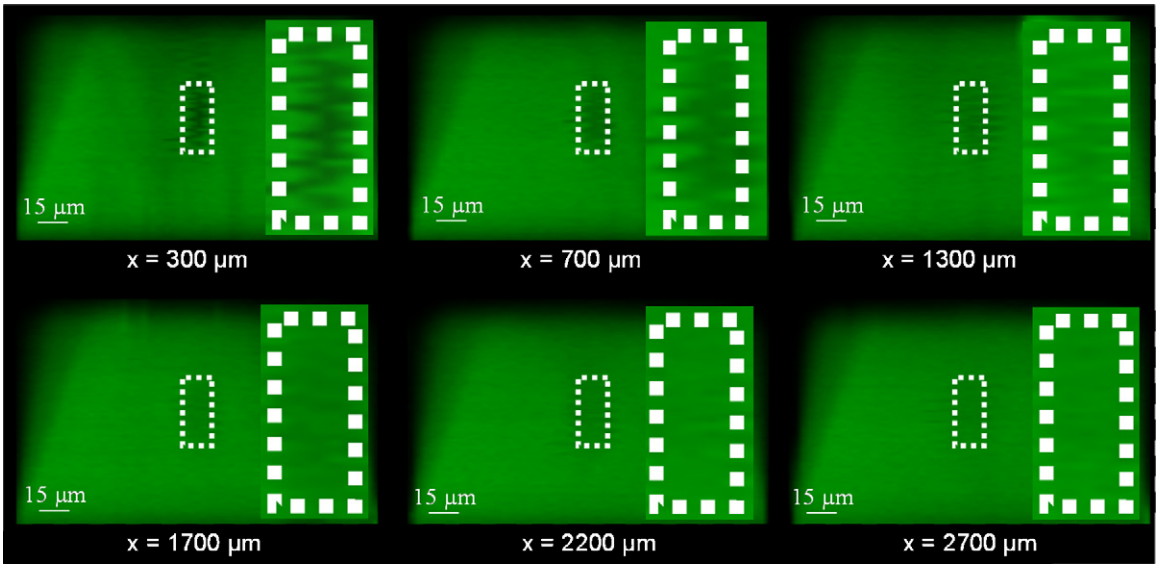

Fig. 3. Example of the CLSM pictures of the cross-section at different positions x, reconstructed from the average intensity on the 30 µm stacks, under the flow rate conditions Qc = 1 µL min^{-1} and Qs = 10 µL min^{-1}. The rectangle with dashed white lines is the ROI determined at the beginning of the main channel and retained for each picture. Insets correspond to the numerical magnification of the ROI.

ing the fluorescent dye though the channel. I_{max} corresponds to the fluorescence intensity in pure water ($W = 1$).

To characterize the dynamic of the mixing, the mixing efficiency and the mixing uniformity were determined as follows.

First, the mixing efficiency (M.E.), which represents the degree of mixing, is:

$$\text{M.E.} = W_{mean} = \frac{I_{mean} - I_{min}}{I_{max} - I_{min}} \quad (2)$$

Second, the mixing uniformity or mixing index (M.I.) is represented by:

$$\text{M.I.} = \frac{\sigma}{W_{mean}} \quad (3)$$

An M.I. below 0.1 indicates that there is efficient mixing in the device.

The evolution of the mixing efficiency versus time is plotted on Fig. 4 at different flow rate conditions.

It can be seen that high mixing efficiency is reached faster for higher focusing ratios (FocRatio = 2Qs/Qc), as the width of the focused stream decreases significantly with this ratio. When two experiments are performed with the same FocRatio, the total volumetric flow rate influences the position along the channel where a desired M.E. is achieved.

The confocal image shows that the stream is mostly focused in two dimensions (Fig. 3). For two-dimensional hydrodynamic focusing, the M.E. versus time was predicted using Fick's law of diffusion ([36], see Eq. (4)). As shown in Fig. 4, the mixing efficiency is well described by the following expression:

$$\text{M.E.} = W_{mean} = \text{erfc}\left(\frac{W_f}{2\sqrt{Dt_{res}}}\right) + \frac{2}{W_f}\sqrt{\frac{Dt_{res}}{\pi}}\left(1 - \exp\left(\frac{W_f^2}{4Dt_{res}}\right)\right) \quad (4)$$

where t_{res} is the residence time, W_f is the width of the focused stream determined at the inlet of the main channel for each experiment, and D is the mutual diffusion coefficient, which is assumed

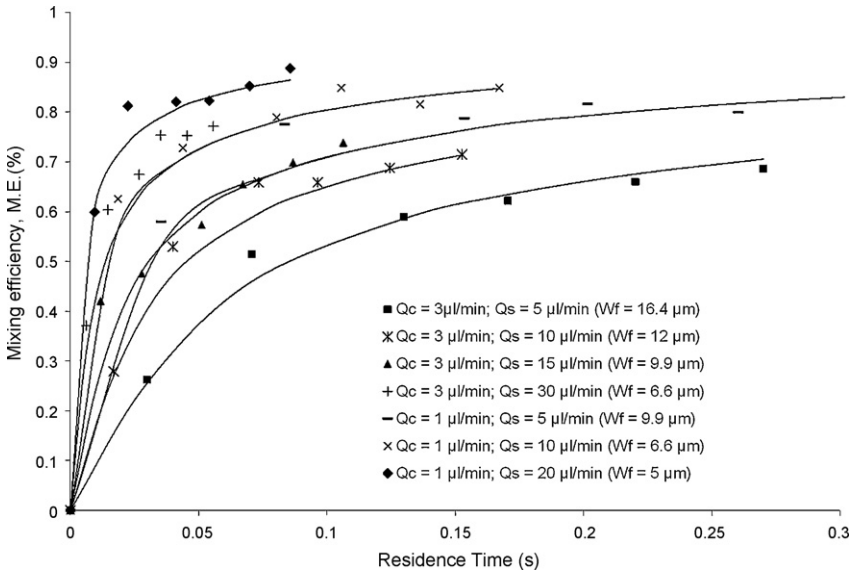

Fig. 4. Mixing efficiency versus time for different operating conditions. Full curves are calculated according to the analytical expression given by Eq. (4). Each experimental set is obtained for a side flow Qs, a capillary flow Qc and is fitted using the measured width W_f.

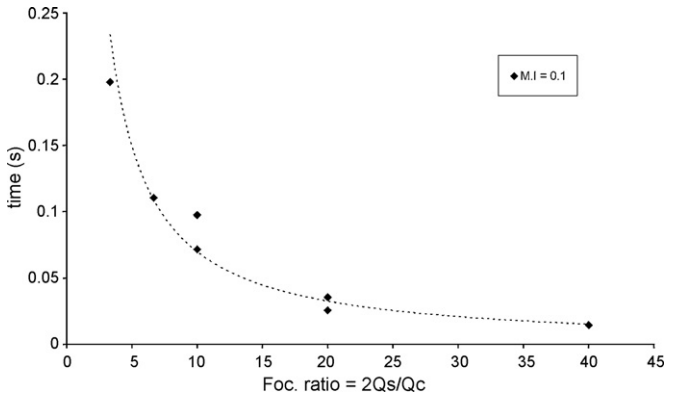

Fig. 5. Time corresponding to a M.I. = 0.1 versus focusing ratio (FocRatio = 2Qs/Qc). The dotted curve through the experimental points is only a guide.

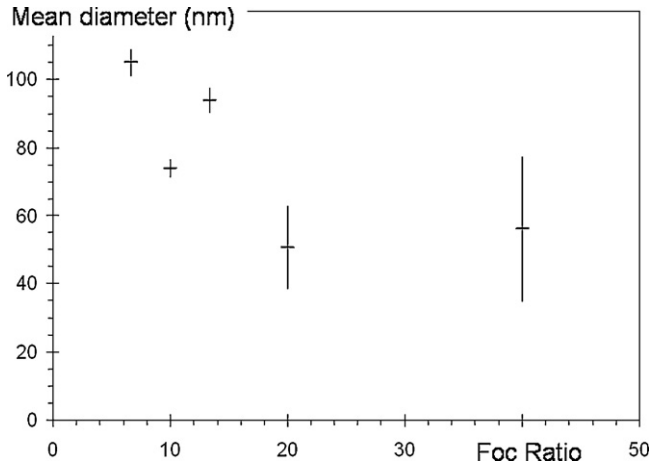

Fig. 6. Mean diameter of the rubrene crystals versus FocRatio (see text). The crystals are obtained under various experimental conditions. The error bar corresponds to the dispersion due to several samples and several analyses on each sample.

constant over the mixing area [38]. This equation is very sensitive to the values of W_f and D. Thus, good agreement between the theoretical and the experimental data was obtained by adjusting the diffusion coefficient D to 3.5×10^{-9} m^2 s^{-1}. This value is similar to the previously reported diffusion coefficient between water and ethanol: 1.25×10^{-9} m^2 s^{-1} at 25 °C [37,38]. The slight difference may be due to the nature of the organic mixture, composed of ethanol and THF instead of pure ethanol. Additionally, the aqueous solution also contains the surfactant, CTACl. Furthermore, as seen in Eq. (4), the diffusion coefficient always appears through the ratio W_f^2/D. The value of D is strongly dependent on the precision of the width measurement. Thus, from these experiments we can conclude that the mixing efficiency in the device depends on the stream width and can be controlled by the focusing ratio, i.e. the volumetric flow rates ratio.

For each set of experiments, we have plotted the time needed to reach a M.I. = 0.1 versus the focusing ratio in Fig. 5.

From this figure, we can deduce that efficient mixing is obtained between 20 and 200 ms. In each case, as the M.I. reaches 0.1, the M.E. is also high, greater than 65% (see Fig. 4), and both values only depend on the focusing ratio. Therefore, as the focusing ratio increases, efficient mixing indexes are reached in a shorter amount of time.

3.2. Synthesis of rubrene nanoparticles

Due to insolubility of rubrene in water, the non-solvent diffusion processes initiate the nucleation of nanoparticles of rubrene, when the concentration of water in the rubrene solution reaches the critical supersaturation of nucleation. The surfactant CTACl, dissolved in water, was necessary to surround the newly generated nanocrystals and to control the growth and size of these crystals [39]. Due to a lower diffusion coefficient than that of parent molecules, the rubrene particles continue to flow in a central focused beam as previously reported [24]. By varying the side and capillary flow rates, the mixing and reacting conditions were varied, which in turn changed the way to obtain supersaturation. In the same Y-type microdevice (see Fig. 1), the side flow rate, Qs, was set at 10 μL min^{-1} and capillary flow rates, Qc, varied between 0.5 and 3 μL min^{-1}. The final concentration of CTACl in the suspensions differed slightly, between 8.7 and 9.9 mmol L^{-1}. For each focusing ratio, between 1 and 4 experiments were performed and the size distribution was measured by DLS. The period of time between the preparation and the analysis could be propitious to the sample ageing, leading to Oswald ripening or aggregation of crystals. Nevertheless no significant change was detected for samples prepared in the same conditions and analysed after 1 or 2 days. The mean diameters of the particles varied from approximately 50 to 110 nm. The size of the nanocrystals is strongly dependent on the focusing ratio. Thus, the larger ratio, for example for 20 and 40, yielded smaller particles.

As seen in Fig. 6, this trend is significant up to a FocRatio of 20, because it shows that the size of the nanocrystals can be predicted by controlling the focusing ratio. The scattering data around each average value may pertain to the time period between the crystallization and the analysis. The fluctuations observed by CLSM, particularly concerning the position of the focused stream in the main channel, may also contribute to this spreading of the data. Furthermore, during some experiments, larger crystals were formed around the silica capillary and recovered in the outlet solution. From the DLS measurements, the appearance of these crystals could also affect the average size of the nanocrystals. New device types, in which a sheath flow is created around the capillary, are being designed to completely eliminate the formation of large crystals in the microdevice [36].

In this crystallization processes, nucleation and growth are governed by the level of supersaturation and the rate to reach this supersaturation level. It is determined from the amount of water that has diffused into the rubrene solution (in an EtOH/THF mixture). In an efficient mixing process, the critical supersaturation needed for nucleation, is reached faster, with proper mixing (low M.I.) in the focused stream. This will then allow for the generation of numerous nuclei whose growth is limited by the amount of available molecules. A larger number of nuclei implies a smaller average size of the particles. Therefore, a higher focusing ratio would lead to smaller particles as shown in Fig. 6.

4. Conclusions

We have shown that the 3D hydrodynamic focusing microdevice is designed to avoid the contact of the crystallizing flow with the channel walls. A higher focusing ratio leads to a more stabilized focused stream, which avoids contact with the channel walls and then prevents unwanted crystal deposition. Concerning the hydrodynamic behaviour, the rectangular shape of the focused stream is due to a likely 2D compression of the capillary flow, and as a result, a 2D model has been applied to the diffusive mixing in the focused stream.

It was then shown that rubrene nanocrystals of controlled size can be synthesized under varied focusing ratios within this 3D hydrodynamic focusing device. A higher focusing ratio reduces the time needed to reach efficient mixing conditions (low M.I., high M.E.). When the supersaturation is obtained more quickly, smaller

particles are obtained by the nucleation and growth processes. The focusing ratio is thought to be the most significant parameter. It is also important to take into account other parameters because the concentrations of the organic molecule and of the surfactant can also influence the particle size. Such studies are in progress on other fluorescent molecules.

Acknowledgments

Callie Croushore thanks the Research Experiences for Undergraduates (REU program) funded by the US National Science Foundation. The authors thank Sylviane Lesieur from the Physico-chimie, Pharmacotechnie, Biopharmacie (CNRS-UMR 8612, Chatenay-Malabry, France) for providing access to the DLS instrument.

References

[1] S. DeWitt, Microreactors for chemical synthesis, Curr. Opin. Chem. Biol. (1999) 350–356.
[2] D. Brown, Synthetic chemistry in microreactors, Chem. Aust. 74 (2007) 14–17.
[3] K.F. Jensen, Microreaction engineering is small better, Chem. Eng. Sci. 56 (2001) 293–303.
[4] B. Bromley, V. Hessel, A. Renken, L. Kiwi-Minsker, "Sandwich reactor" for heterogeneous catalytic processes: N_2O decomposition as a case study, Chem. Eng. Technol. 31 (2008) 1162–1169.
[5] A. Jahn, J.E. Reiner, W.N. Vreeland, D.L. DeVoe, L.E. Locascio, M. Gaitan, Preparation of nanoparticles by continuous-flow microfluidics, J. Nanopart. Res. 10 (2008) 925–934.
[6] C.H. Chang, B.K. Paul, V.T. Remcho, Synthesis and post-processing of nanomaterials using microreaction technology, J. Nanopart. Res. 10 (2008) 965–980.
[7] W. Ehrfeld, V. Hessel, H. Löwe, Microreactors: New Technology for Modern Chemistry, Wiley VCH Verlag, Weinheim, 2000.
[8] A.J. deMello, Control and detection of chemical reactions in microfluidic systems, Nature 442 (2006) 394–402.
[9] Y. Song, J. Hormes, C.S.S.R. Kumar, Microfluidic synthesis of nanomaterials, Small 4 (2008) 698–711.
[10] H. Nakamura, Y. Yamaguchi, M. Miyazaki, Preparation of CdSe nanocrystals in a micro-flow-reactor, Chem. Commun. 23 (2002) 2844–2845.
[11] S. Marre, J. Park, J. Rempel, J. Guan, M.G. Bawendi, K.F. Jensen, Supercritical continuous-microflow synthesis of narrow size distribution quantum dots, Adv. Mater. 20 (2008) 4830–4834.
[12] P.H. Mugdur, Y.J. Chang, S.Y. Han, A comparison of chemical bath deposition of CdS from a batch reactor and a continuous-flow microreactor, J. Electrochem. Soc. 154 (2007) D482–D488.
[13] L.H. Hung, K.M. Choi, W.Y. Tseng, Y.C. Tan, K.J. Sheab, A.P. Lee, Alternating droplet generation and controlled dynamic droplet fusion in microfluidic device for CdS nanoparticles synthesis, Lab. Chip 6 (2006) 174–178.
[14] J.D. Winterton, D.R. Myers, J.M. Lippmann, A novel continuous microfluidic reactor design for the controlled production of high-quality semiconductor nanocrystals, J. Nanopart. Res. 10 (2008) 893–905.
[15] E.M. Chan, P. Alivisatos, R.A. Mathies, High-temperature microfluidic synthesis of CdSe nanocrystals in nanoliter droplets, J. Am. Chem. Soc. 127 (2005) 13854–13861.
[16] E.M. Chan, R.A. Mathies, A.P. Alivisatos, Size-controlled growth of CdSe nanocrystals in microfluidic reactors, Nano Lett. 3 (2003) 199–201.
[17] Y. Song, C.S.S.R. Kumar, J. Hormes, Synthesis of palladium nanoparticles using a continuous flow polymeric microreactor, J. Nanosci. Nanotechnol. 4 (2004) 788–793.
[18] Y. Song, E.E. Doomes, J. Prindle, R. Tittsworth, J. Hormes, C.S.S.R. Kumar, Investigations into sulfobetaine-stabilized Cu nanoparticles formation: toward development of a microfluidic synthesis, J. Phys. Chem. B 109 (2005) 330–338.
[19] J. Wagner, J.M. Kohler, Continuous synthesis of gold nanoparticles in a microreactor, Nano Lett. 5 (2005) 4685–4691.
[20] J. Kohler, J.M. Wagner, J. Albert, Formation of isolated and clustered Au nanoparticles in the presence of polyelectrolyte molecules using a flow-through Si chip reactor, J. Mater. Chem. 15 (2005) 1924–1930.
[21] S.A. Khan, A. Gunther, M.A. Schmidt, K.F. Jensen, Microfluidic synthesis of colloidal silica, Langmuir 20 (2004) 8604–8611.
[22] A. Jahn, W.N. Vreeland, M. Gaitan, L.E. Locascio, Controlled vesicle self-assembly in microfluidic channels with hydrodynamic focusing, J. Am. Chem. Soc. 126 (2004) 2674–2675.
[23] K.C. Popat, T.A. Desai, Poly(ethylene glycol) interfaces: an approach for enhanced performance of microfluidic systems, Biosens. Bioelectron. 19 (2004) 1037–1044.
[24] S. Desportes, Z. Yatabe, S. Baumlin, V. Génot, J.P. Lefèvre, H. Ushiki, J.A. Delaire, R.B. Pansu, Fluorescence lifetime imaging microscopy for in situ observation of the nanocrystallization of rubrene in a microfluidic set-up, Chem. Phys. Lett. 446 (2007) 212–216.
[25] A.A. Hassan, O. Sandre, V. Cabuil, P. Tabeling, Synthesis of iron oxide nanoparticles in a microfluidic device: preliminary results in a coaxial flow millichannel, Chem. Commun. 1783 (2008) 1783–1785.
[26] S.A. Pabit, S.J. Hagen, Laminar-flow fluid mixer for fast fluorescence kinetics studies, J. Biophys. 83 (2002) 2872–2878.
[27] J.B. Knight, A. Vishwanath, J.P. Brody, R. Austin, Hydrodynamic focusing on a silicon chip: mixing nanoliters in microseconds, Phys. Rev. Lett. 80 (1998) 3863–3866.
[28] S.R. Forrest, The path to ubiquitous and low-cost organic electronic appliances on plastic, Nature 428 (2004) 911–917.
[29] B.D. Chapma, A. Checco, R. Pindak, T. Siegrist, C. Kloc, Dislocations and grain boundaries in semiconducting rubrene single-crystals, J. Crystal Growth 290 (2006) 479–484.
[30] S. Chung, S.J. Park, J.K. Kim, C. Chung, D.C. Han, J.K. Chang, Plastic microchip flow cytometer based on 2- and 3-dimensional hydrodynamic flow focusing, Microsyst. Technol. 9 (2003) 525–533.
[31] E. Destandau, J.P. Lefèvre, A. Chouai Fakhr Eddine, S. Desportes, I. Leray, J.A. Delaire, A novel microfluidic flow-injection analysis device with fluorescence detection for cation sensing, Anal. Bioanal. Chem. 387 (2007) 2627–2632.
[32] J.F. Liu, G. Min, W.A. Ducker, AFM study of absorption of cationic surfactants and cationic polyelectrolytes at the silica–water interface, Langmuir 17 (2001) 4895–4903.
[33] M.M. Martin, L. Lindqvist, The pH dependence of fluorescein fluorescence, J. Lumin. 10 (1975) 381–390.
[34] M. Martinelli, V. Viktorov, Modelling of laminar flow in the inlet section of rectangular microchannels, J. Micromech. Microeng. 19 (2009) 025013.
[35] P. Galambos, F.K. Forster, Micro-fluidic diffusion coefficient measurement, in: Micro Total Analysis Systems'98, 1998, pp. 189–192.
[36] H.Y. Park, X. Qiu, E. Rhoades, J. Korlach, L.W. Kwok, W.R. Zipfel, W.W. Webb, L. Pollack, Achieving uniform mixing in a microfluidic device: hydrodynamic focusing prior to mixing, Anal. Chem. 78 (2006) 4465–4473.
[37] P.W. Atkins, Physical Chemistry, Oxford Press, 1992.
[38] K.C. Pratt, W.A. Wakeham, The mutual diffusion coefficient of ethanol–water mixtures: determination by a rapid, new method, Proc. R. Soc. Lond. A 336 (1974) 393–406.
[39] H. Lannibois, A. Hasmy, R. Botet, O. Aguerre Charriol, B. Cabane, Surfactant limited aggregation of hydrophobic molecules in water, J. Phys. II 2 (1997) 319–342.